
DQ-DETR: DETR WITH DYNAMIC QUERY FOR TINY OBJECT DETECTION

Yi-Xin Huang

National Yang Ming Chiao Tung University
svkatie.nctu.ee08@nycu.edu.tw

Hou-I Liu

National Yang Ming Chiao Tung University
k39967.c@nycu.edu.tw

Hong-Han Shuai

National Yang Ming Chiao Tung University
hhshuai@nycu.edu.tw

Wen-Huang Cheng

National Taiwan University
wenhuang@csie.ntu.edu.tw

ABSTRACT

Despite previous DETR-like methods having performed successfully in generic object detection, tiny object detection is still a challenging task for them since the positional information of object queries is not customized for detecting tiny objects, whose scale is extraordinarily smaller than general objects. Also, DETR-like methods using a fixed number of queries make them unsuitable for aerial datasets, which mostly contain tiny objects, and the numbers of instances are imbalanced between different images. Thus, we present a simple yet effective model, DQ-DETR, consisting of three components: categorical counting module, counting-guided feature enhancement, and dynamic query selection to solve the above-mentioned problems. DQ-DETR uses the prediction and density maps from the categorical counting module to dynamically adjust the number and positional information of object queries. Our model DQ-DETR outperforms previous CNN-based and DETR-like methods, achieving state-of-the-art mAP 30.2% on the AI-TOD-V2 dataset, which mostly consists of tiny objects.

Keywords DETR · Tiny Object Detection

1 Introduction

Convolutional neural networks (CNNs) are superior to processing the RGB semantic and spatial texture features. Most object detection methods are primarily based on CNNs. For example, Faster R-CNN [1] introduces a region proposal network to generate potential object regions. FCOS [2] apply a center prediction branch to increase the quality of the bounding boxes.

However, CNNs are unsuitable for attaining long-range dependency in the image, restricting the detection performance. Recently, DETR [3] incorporates CNN and transformer architecture to establish a new object detection framework. DETR utilizes the transformer encoder to integrate the partition image patches and pass them with the learnable object queries to the transformer decoder for final detection results. Moreover, a series of DETR-like methods [4, 5, 6, 7] aim to advance DETR performance and accelerate DETR convergence speed. For example, Deformable-DETR [4] uses multi-scale feature maps to improve its ability to detect different sizes of objects. Also, the use of deformable attention modules can not only capture more informative and contextually relevant features but accelerate training convergence as well.

We argue that the previous DETR-like methods are inappropriate in aerial images, which only contain tiny objects and have an imbalance of instances between different images. In the previous DETR-like methods, the object queries used in the transformer decoder do not consider the number and position of instances in the image. Generally, they apply the fixed number K of object queries, where K represents the maximum number of the detection objects, e.g., $K=100$, 900 in DETR and DINO-DETR, respectively. DETR [3] and Deformable-DETR [4] apply a fixed number of sparse queries, suffering a low recall rate. To address the problem, DDQ [8] select dense distinct queries, $K=900$, with a class-agnostic

Table 1: Comparison of DETR-like models’ queries strategy under different situations.

	Sparse	Dense	Imbalance	Characteristics
Deformable DETR [4]	✓			Sparse Queries (K=300) with One-To-One Assignment; Low Recall
DDQ-DETR [8]	✓	✓		Dense Distinct Queries (K=900); Low Recall if #Object \gg #Query
DQ-DETR(Ours)	✓	✓	✓	Dynamically adjust the "Number" and "Position" of Queries

NMS based on a hand-designed IoU threshold. Though DDQ applies dense queries for detection, the number of queries is still limited.

The fixed number of queries will cause low detection accuracy in aerial datasets since the number of objects may vary drastically in different images. In the AI-TOD-V2 dataset [9], some images have more than 1500 objects, but others have less than 10 objects. Under the situation that the number of objects in images is more than the DETR’s query number K, a low recall rate is an expected issue. Using smaller K restricts the recall of the objects in dense images, leaving lots of instances undetected (FN). While using a large K in the sparse images not only introduces many underlying false positive samples (FP) but also causes a waste of computing resources since the computing complexity in the decoder’s self-attention modules grows quadratic with the number of queries K.

Besides, in the previous DETR-like methods, the object queries used in the transformer decoder do not consider the position of instances in the image. The position of object queries is a set of learned embeddings, which are irrelevant to the current image and do not have explicit physical meaning to tell where the queries are focusing on. The static positions of object queries are unsuitable for aerial datasets, where the distribution of instances varies extremely in different images, i.e., some images contain dense objects concentrated in specific areas, while some only have a few objects scattered throughout the images.

Stemming on the above-mentioned weakness, we proposed a novel DETR-like method named DQ-DETR which mainly focuses on dynamically adapting the numbers of queries and enhancing the position of queries to locate the tiny objects precisely. In this work, we propose a dynamic query selection module for adaptively choosing different numbers of object queries in DETR’s decoder stage, resulting in fewer FP in sparse images and fewer FN in dense images. Moreover, we generate the density maps and estimate the number of instances in an image by the categorical counting module. The number of object queries is adjusted based on the predicted counting number. In addition, we aggregate the density maps with the visual feature from the transformer encoder to reinforce the foreground features, enhancing the spatial information for tiny objects. The strengthened visual feature will be further used to improve the positional information of object queries. As such, we can simultaneously handle the images with few and crowded tiny objects by dynamically adjusting the number and position of object queries used in the decoder.

In summary, our contributions are summarized as follows:

1. We point out the crucial limitation of previous DETR-like methods that make them unsuitable for aerial image datasets.
2. Experimental result shows that our proposed DQ-DETR significantly surpasses the state-of-the-art method by 16.6%, 20.5% in terms of AP, AP_{vt} on the AI-TOD-V2 dataset.
3. We design a simple yet accurate categorical counting module to guide the number of object queries effectively. In addition, we enhance the transformer’s visual feature with a density map to improve the positional information of object queries.

2 Related work

2.1 DETR-like Methods.

DETR [3] proposes an end-to-end object detection framework based on the transformer named DETR (DEtection TRansformer), where the transformer encoder extracts instance-level features from an image, and the transformer decoder uses a set of learnable queries to probe and pool features from images. While DETR achieves comparable results with the previous classical CNN-based detectors [1, 2], it suffers severely from the problem of slow training convergence, needing 500 epochs of training to perform well. Many follow-up works have attempted to address the slow training convergence of DETR from different perspectives.

Some point out that the cause of DETR’s slow convergence is due to the unstable Hungarian matching and the cross-attention mechanism in the transformer decoder. [10] proposes an encoder-only DETR, discarding the transformer

decoder. Dynamic DETR [11] designs an ROI-based dynamic attention mechanism in the decoder that can focus on regions of interest from a coarse-to-fine manner. Deformable-DETR [4] proposes an attention module that only attends to a few sampling points around a reference point. DN-DETR [5] introduces denoising training to reduce the difficulty of bipartite graph matching.

Another series of works makes improvements in decoder object queries. Since the object queries are just a set of learnable embedding in DETR [3], [7, 12, 13] imputes the slow convergence of DETR to the implicit physical explanation of object queries. Conditional DETR [13] decouples the decoder’s cross-attention formulation and generates conditional queries based on reference coordinates. DAB-DETR [7] formulates the positional information of object queries as 4-D anchor boxes (x, y, w, h) that are used to provide ROI (Region of Interest) information for probing and pooling features.

2.2 Tiny Object Detection.

Detecting small objects is challenging due to their lack of pixels. Early works apply data augmentation to oversample the instance of tiny objects. For example, [14], copy-paste small objects into the same image. [15] proposes a K sub-policies that automatically transform features from the instance level. In addition, several approaches, such as [9, 16, 17, 18] indicate that traditional Inter Section Union (IoU) metrics are ill-suited for tiny objects. When the object size difference is significant, IoU becomes highly sensitive. To design the appropriate metrics for the tiny object, DotD [18] considers the object’s absolute and relative size to formulate a new loss function. [16, 17, 18] design a new label assignment based on Gaussian distribution, which alleviates the sensitivity of the object size.

However, these methods highly rely on the predefined threshold, which is unstable to a different dataset. Instead, our DQ-DETR uses a counting-guided feature enhancement module to improve the visual features with more spatial information about tiny objects’ scale and location. Also, although the above-mentioned DETR-like methods have improved the formulation of queries, they are not specially designed to detect tiny objects. For example, the object queries in [3, 5, 7, 13] are learned from the training data and remain the same for different input images. Our proposed DQ-DETR is the first DETR-like model that focuses on tiny object detection. DQ-DETR dynamically adjusts the number of object queries and enhances the position information of queries in order to detect tiny objects precisely under imbalanced situations in aerial datasets.

3 Method

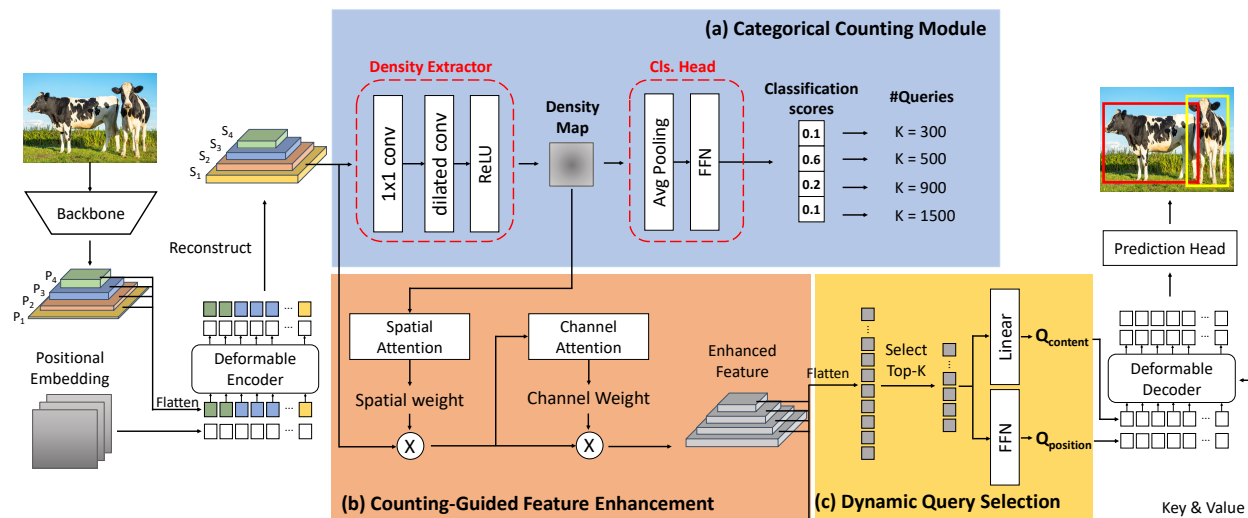


Figure 1: Overall architecture of our method. (a) Categorical Counting module, which classifies the number of instances in images into 4 levels. (b) Counting-Guided Feature Enhancement, which refines the encoder’s visual feature with a density map. (c) Dynamic Query Selection, which dynamically adjusts the number of queries and enhances the content and position of queries.

3.1 Overview

The overall structure of DQ-DETR is shown in Fig. 1. As a DETR-like method, DQ-DETR is an end-to-end detector that contains a CNN backbone, a deformable transformer encoder [4], a deformable transformer decoder [4], and several prediction heads. We further implement a new categorical counting module, a counting-guided feature enhancement module, and dynamic query selection based on DETR’s architecture. Given an input image, we first extract multi-scale features with a CNN backbone and feed them into the transformer encoder to attain the encoder’s visual feature. Afterward, our categorical counting module determines how many object queries are used in the transformer decoder, as shown in Fig. 1(a). Besides, we propose a novel counting-guided feature enhancement module, shown in Fig. 1(b), to strengthen the encoder’s visual feature with spatial information of tiny objects. Last, the positional information of object queries will be refined via dynamic query selection, shown in Fig. 1(c). The following section will describe the proposed Categorical Counting module, Counting-Guided Feature Enhancement, and Dynamic Query Selection.

3.2 Reconstruction of Encoder’s Feature Map

Following DETR’s pipeline, we use multi-scale feature maps $P_i \in \{1, 2, \dots, l\}$ extracted from different stages of the backbone as the input of the transformer encoder. To form the input sequence of the transformer encoder, we flatten each layer of multi-scale feature maps P_i from $\mathbb{R}^{d \times h_i \times w_i}$ to $\mathbb{R}^{d \times h_i w_i}$ and then concatenate them together. The higher resolution feature contains more spatial details, which is beneficial to object counting and detecting tiny objects.

In our proposed categorical counting module, we will perform convolution operation on the transformer encoder features. Hence, we reconstruct the flattened encoder’s multi-scale visual features by reshaping its spatial dimension, resulting in 2-D feature maps $S_i \in \mathbb{R}^{d \times h_i \times w_i}$. We denote the reconstructed encoder’s multi-scale visual features as EMSV features for brevity.

3.3 Categorical Counting Module

The categorical counting module aims to estimate the number of objects in the images. It consists of a density extractor and a classification head.

3.3.1 Density Extractor.

We take the largest feature map S_1 of the EMSV features and generate the density map F_c through the density extractor. The input feature map S_1 is firstly fed into a 1×1 convolution layer for channel reduction ($\mathbb{R}^{b \times 256 \times h \times w} \rightarrow \mathbb{R}^{b \times 512 \times h \times w}$). Then, it is sent into a series of dilated convolution layers to acquire a density map F_c , which contains counting-related information. Specifically, dilated convolution layers enlarge the receptive field and capture rich long-range dependency for tiny objects.

3.3.2 Counting Number Classification.

Lastly, we estimate the counting number N , i.e., the number of instances per image, by a classification head and categorize them into four levels, which are $N \leq 10$, $10 < N \leq 100$, $100 < N \leq 500$, and $N > 500$. The classification head consists of two linear layers. Further, the numbers 10, 100, and 500 are selected based on the dataset’s characteristics, i.e., the mean and standard deviation of the number of instances N per image. Notably, we do not use the regression head as in the traditional crowd-counting methods, which regresses the counting number to a specific number. We attribute the reason to the drastic difference of the number of instances in each image, where N ranges from 1 to 2267 in different images of AI-TOD-V2. It is difficult to regress an accurate number, hurting the detection performance.

3.4 Counting-Guided Feature Enhancement Module (CGFE)

The EMSV feature will be refined with the density map from the categorical counting module through the proposed Counting-Guided Feature Enhancement Module (CGFE) to improve the spatial information of tiny objects. The refined features will further be used to enhance the position information of queries. This module comprises a spatial cross-attention and a channel attention operations.

3.4.1 Spatial cross-attention map.

To utilize the abundant spatial information in the density map F_c , a 2-D cross-spatial attention is calculated. We employ a 1×1 convolution layers to down-sample the density map F_c , creating multi-scale counting feature maps

$F_{c,i} \in \{1, 2, \dots, l\}$ to in line with the shape of each layer of encoder’s multi-scale feature maps $S_i \in \{1, 2, \dots, l\}$. Subsequently, we first apply average pooling (AvgP.) and max pooling (MaxP.) on each layer of multi-scale counting features $F_{c,i} \in \mathbb{R}^{b \times 256 \times h \times w}$ along the channel axis. Then, the two pooling features $\mathbb{R}^{b \times 1 \times h \times w}$ are concatenated and sent into a 7x7 convolution layer followed by a Sigmoid function to produce spatial attention map $W_s \in \mathbb{R}^{b \times 1 \times h \times w}$. We formulate this process in Eq. 1.

Since the density maps F_c contain the location and density information about the object, the spatial attention maps generated by them can focus on the important region, i.e., foreground objects, and enhance the EMSV feature with abundant spatial information.

$$W_{s,i} = \sigma \left(Conv_{7 \times 7} \left(Concat \begin{matrix} AvgP.(Conv_{1 \times 1}(F_{c,i})) \\ MaxP.(Conv_{1 \times 1}(F_{c,i})) \end{matrix} \right) \right). \quad (1)$$

The generated spatial attention map $W_{s,i}$ multiplies with EMSV feature S_i element-wisely and further obtain the spatial-intensified features E_i , as shown in Eq. 2.

$$E_i = W_{s,i} \otimes S_i, \quad (2)$$

3.4.2 Channel attention map.

After the spatial cross-attention, we further apply 1-D channel attention to the spatial-intensified features E_i , exploiting the inter-channel relationship of features. Specifically, we first apply average pooling and max pooling on each layer of $E_i \in \mathbb{R}^{b \times 256 \times h \times w}$ along the spatial dimension. Next, the two pooling features $\mathbb{R}^{b \times 256 \times 1 \times 1}$ are sent into a shared MLP and merged together with element-wise addition to create channel attention map $W_{c,i}$. Finally, the channel attention map $W_{c,i} \in \mathbb{R}^{b \times 256 \times 1 \times 1}$ is multiplied with original $E_i \in \mathbb{R}^{b \times 256 \times h \times w}$ and further get the counting-guided intensified feature maps F_t . The formulas are defined in Eq. 3 and Eq. 4:

$$W_{c,i} = \sigma(MLP(AvgP.(E_i)) + MLP(MaxP.(E_i))), \quad (3)$$

$$F_{t,i} = W_{c,i} \otimes E_i. \quad (4)$$

3.5 Dynamic Query Selection

3.5.1 Number of queries.

In dynamic query selection, we firstly use the classification result from the categorical counting module to determine the number of queries K used in the transformer decoder. The four classification classes in the categorical counting module correspond to four distinct numbers of queries, which are $K = 300, 500, 900,$ and 1500 , i.e., if the image is classified as $N \leq 10$, we will use $K = 300$ queries in the further detection task, and so forth.

3.5.2 Enhancement of queries.

For queries formulation, we follow the idea of DAB-DETR [7], where the queries are composed of content and positional information. The content of queries is a high-dimension vector, while the position of queries is formulated as a 4-D anchor box (x, y, w, h) to accelerate training convergence.

Further, we use the intensified multi-scale feature maps F_t from the previous CGFE module to improve the content $Q_{content}$ and position $Q_{position}$ of queries. The each layer of F_t are firstly flattened into pixel level and concatenate together, forming $F_{flat} \in \mathbb{R}^{b \times 256 \times hw}$. The top-K features will be selected as priors to enhance decoder queries, where K is the number of queries used in the transformer decoder stage. The selection is based on the classification score. We feed F_{flat} into an FFN for the object classification task and generates the classification score $\in \mathbb{R}^{b \times m \times hw}$, where m is the number of object classes in the dataset. Afterwards, we will generate the content and position of queries using the selected top-K features F_{select} .

$$\begin{aligned} Score &= FFN(F_{flat}), \\ F_{select} &= topK_{Score}(F_{flat}). \end{aligned} \quad (5)$$

The content of queries is generated by a linear transform of the selected features F_{select} . As for the position of queries, we use an FFN to predict bias $\hat{b}_i = (\Delta b_{ix}, \Delta b_{iy}, \Delta b_{iw}, \Delta b_{ih})$ to refine the original anchor boxes. Let $(x, y)_i$ index a selected feature from multi-level features $F_t \in \{1, 2, \dots, l\}$ at position (x, y) . The selected feature has its original anchor box (x_i, y_i, w_i, h_i) as the position prior of queries, where (x_i, y_i) are normalized coordinates $\in [0, 1]^2$ and

(w_i, h_i) are setting related to the scale of feature F_t . The predicted bias $\hat{b}_i = (\Delta b_{ix}, \Delta b_{iy}, \Delta b_{iw}, \Delta b_{ih})$ are then added to original anchor box to refine the position of object queries.

$$\begin{aligned} Q_{content} &= \text{Linear}(F_{select}), \\ Q_{position,bias} &= \text{FFN}(F_{select}). \end{aligned} \quad (6)$$

Since the features F_{select} are selected from F_t , which is generated from the previous CGFE module, they contain abundant scale and location information of tiny objects. Hence, the enhanced content and position of object queries are tailored based on each image’s crowded or sparse situation and make the queries easier to localize the tiny objects in transformer decoder stage.

3.6 Overall Objective

3.6.1 Hungarian Loss

Based on DETR [3], we use a Hungarian algorithm to find an optimal bipartite matching between ground truth and prediction and optimize losses. The Hungarian loss consists of L1 loss and GIoU loss [19] for bounding box regression and focal loss [20] with $\alpha = 0.25, \gamma = 2$ for classification task, which can be denoted as Eq. 7. Follow the settings of DAB-DETR [7], we use $\lambda_1 = 5, \lambda_2 = 2, \lambda_3 = 1$ in our implementation.

$$L_{hungarian} = \lambda_1 L_1 + \lambda_2 L_{GIoU} + \lambda_3 L_{focal}. \quad (7)$$

In addition, we use the cross entropy loss in the categorical counting module to supervise the classification task. Further, Hungarian losses are also applied as the auxiliary losses for each decoder stage. The overall loss can be denoted as Eq. 8.

$$L_{total} = L_{hungarian} + L_{aux} + L_{counting}. \quad (8)$$

4 Experiments

4.1 Dataset

To demonstrate the effectiveness of our model, we conduct experiments on the aerial dataset AI-TOD-V2 [9], which mostly consists of tiny objects.

AI-TOD-V2. This dataset includes 28,036 aerial images with 752,745 annotated object instances. There are 11,214 images for the train set, 2,804 for the validation set, and 14,018 for the test set. The average object size in AI-TOD-V2 is only 12.7 pixels, with 86% of objects in the dataset smaller than 16 pixels, and even the largest object is no bigger than 64 pixels. Also, the number of objects in an image can vary enormously from 1 to 2667, where the average number of objects per image is 24.64 with a standard deviation of 63.94.

Evaluation Metric. We use the AP (Average Precision) metric with a max detection number of 1500 to evaluate the performance of our proposed method. Specifically, AP means the average value from $AP_{0.5}$ to $AP_{0.95}$, with IoU interval of 0.05. Moreover, AP_{vt} , AP_t , AP_s , and AP_m are for very tiny, tiny, small, and medium scale evaluation in AI-TOD [21].

4.2 Implementation Details

Based on the DETR-like structure, we use a 6-layer transformer encoder, a 6-layer transformer decoder with 256 as the hidden dimension, and a ResNet50 as our CNN backbone. Furthermore, we train our model for 24 epochs with Adam optimizer and weight decay 0.0001 using 2 NVIDIA 3090 GPUs. The batch size is set to 1 due to memory constraints. The same random crop and scale augmentation strategies are applied following DETR [3]. Also, we apply a two-stage training scheme. We first train the categorical counting module to achieve more stable results for the number of queries in the transformer decoder. After stabilizing the counting result, we add the counting-guided feature enhancement module into training to refine the encoder’s visual features with density maps.

4.3 Main Results on AI-TOD-V2

Table 2 shows our main results on the AI-TOD-V2 test split. We compare the performances of our DQ-DETR with strong baselines, including both CNN-based and DETR-like methods. All CNN-based methods except YOLOv3 use

Table 2: **Experiments on AI-TOD-V2.** All models are trained on the *trainval* split and evaluated on the *test* split. * denotes a re-implementation of the results with the same experiment setting.

Method	#Epochs	Backbone	AP	AP ₅₀	AP ₇₅	AP _{vt}	AP _t	AP _s	AP _m
CNN-based models									
YOLOv3 [22]	12	Darknet53	4.1	14.6	0.9	1.1	4.8	7.7	8.0
RetinaNet [20]	12	ResNet50-FPN	8.9	24.2	4.6	2.7	8.4	13.1	20.2
Faster-RCNN [1]	12	ResNet50-FPN	12.8	29.9	9.4	0.0	9.2	24.6	37.0
Cascade R-CNN [23]	12	ResNet50-FPN	15.1	34.2	11.2	0.1	11.5	26.7	38.5
DetectoRS [24]	12	ResNet50-FPN	16.1	35.5	12.5	0.1	12.6	28.3	40.0
DotD [18]	12	ResNet50-FPN	20.4	51.4	12.3	8.5	21.1	24.6	30.4
NWD-RKA [9]	12	ResNet50-FPN	24.7	57.4	17.1	9.7	24.2	29.8	39.3
RFLA [17]	12	ResNet50-FPN	25.7	58.9	18.8	9.2	25.5	30.2	40.2
DETR-like models									
DETR-DC5* [3]	200	ResNet50	10.4	32.5	3.9	3.6	9.3	13.2	24.6
Deformable-DETR* [4]	50	ResNet50	18.9	50.0	10.5	6.5	17.6	25.3	34.4
DAB-DETR* [7]	50	ResNet50	22.4	55.6	14.3	9.0	21.7	28.3	38.7
DINO-DETR* [6]	24	ResNet50	25.9	61.3	17.5	12.7	25.3	32.0	39.7
DQ-DETR(Ours)	24	ResNet50	30.2(+4.3)	68.6	22.3	15.3	30.5	36.5	44.6

ResNet50 with feature pyramid network (FPN) [25]. Moreover, since there is no previous research of DETR-like models on tiny object detection, our DQ-DETR is the first DETR-like model that focuses on detecting tiny objects. We re-implement a series of DETR-like models on AI-TOD-V2, and all DETR-like methods except DETR use 5 scales of feature maps with deformable attention [4]. For 5-scale feature maps, features are extracted from stages 1, 2, 3, and 4 of the backbone, and add the extra feature by down-sampling the output of stage 4.

The results are summarized in Table 2, our proposed DQ-DETR achieves the best result **30.2** AP compared with other state-of-the-art methods, including CNN-based and DETR-like methods. Also, DQ-DETR surpasses the baseline by 20.5%, 20.6%, 14.1%, and 12.3% in terms of AP_{vt}, AP_t, AP_s, AP_m. The performance gain is greater on AP_{vt}, and AP_t, and our DQ-DETR outperforms the advanced series of DETR-like models on AI-TOD-V2. We credit the performance gains for the following reasons: (1) DQ-DETR fuses the transformer visual features with a density map from the categorical counting module to improve the positional information of object queries, which makes the queries more suitable for localizing tiny objects. (2) Our dynamic query selection adaptively chooses an adequate number of object queries used for the detection task and can handle the images with either few or crowded objects.

Table 3: **Experiments on VisDrone.** All models are trained on the *train* split and evaluated on the *val* split. * denotes a re-implementation of the results with the same experiment setting.

Model	AP	AP ₅₀	AP ₇₅
Faster R-CNN [1]	21.4	40.7	19.9
Cascade R-CNN [23]	22.6	38.8	23.2
Yolov5 [26]	24.1	44.1	22.3
CEASC [27]	28.7	50.7	24.7
SDP [28]	30.2	52.5	28.4
DINO-DETR* [6]	35.8	58.3	36.8
DQ-DETR (Ours)	37.0	60.9	37.9

4.4 Results on VisDrone

Besides AI-TOD-V2, we also conduct experiments on the VisDrone [29] dataset to demonstrate the effectiveness of our model DQ-DETR. **VisDrone.** This dataset includes 14,018 drone-shot images, with 6,471 images for the train set, 548 for the validation set, and 3,190 for the test set. There are 10 categories, and the image resolution is 2000 × 1500 pixels.

Also, the images are diverse in a wide range of aspects, including objects (pedestrians, vehicles, bicycles, etc.) and density (sparse and crowded scenes), where the average number of objects per image is 40.7 with a standard deviation of 46.41.

Table 3 shows our results on the VisDrone *val* split. We compare the performances of our DQ-DETR with other methods. Our proposed DQ-DETR achieves the best result **37.0** AP compared with other state-of-the-art methods, including CNN-based and DETR-like methods. Also, DQ-DETR surpasses the baseline DINO-DETR by 1.2, 2.6, and 1.1 in terms of AP, AP_{50} , AP_{75} .

4.5 Ablation Study

Categorical counting, counting-guided feature enhancement, and dynamic query selection are the newly proposed contributions. We conduct a series of ablation studies to verify the effectiveness of each component proposed in this paper. DINO-DETR is chosen as the comparing DETR-like baseline.

4.5.1 Main ablation experiment.

Table 4 shows the performance of our contributions separately on AI-TODv2. The results demonstrate that each component in DQ-DETR contributes to performance improvement. We attain an improved +2.2 AP over the baseline with the categorical counting module and dynamic query selection. Furthermore, with feature enhancement refining the encoder’s feature, it gains an extra improvement of +4.3, +2.6, +5.2 on AP, AP_{vt} , and AP_t over the baseline. Besides, the experiment with the counting module and feature enhancement together but without dynamic query selection further shows that introducing an additional counting-guided feature-enhancing task improves performance, even when query numbers remain static. Consequently, we prove the power of each component in DQ-DETR on AI-TOD-V2.

Table 4: Overall ablation for our architecture on AI-TOD-V2 *test* split.

Categorical Counting (CC)	Dynamic Query Selection (DQS)	Feature Enhancement (FE)	AP	AP_{vt}	AP_t	AP_s	AP_m
			25.9	12.7	25.3	32.0	39.7
✓	✓		28.1	12.3	27.8	34.6	44.1
✓		✓	29.1	14.4	29.3	35.2	44.1
✓	✓	✓	30.2	15.3	30.5	36.5	44.6

4.5.2 Ablation of DQ-DETR with different number of instances in images.

We explore our DQ-DETR’s performance under different numbers of instances in an image. We classify the AI-TOD-V2 dataset into 4 levels based on the number of instances N in the image as in the categorical counting module, i.e., $N \leq 10$, $10 < N \leq 100$, $100 < N \leq 500$, and $500 < N$. Our proposed DQ-DETR’s performance is analyzed under these four situations. The results are shown in Table 5 compared with DINO-DETR as the baseline. Our DQ-DETR dynamically adjusts the number of object queries based on the number of instances in the image. while DINO-DETR always uses 900 queries in all situations.

We can observe that in the situations of $N \leq 10$, and $10 < N \leq 100$, our DQ-DETR uses fewer numbers of queries and outperforms the baseline by 16%, and 16.4% in terms of AP. The performances in terms of AP_{vt} , AP_t surpass the baseline by 19.8%, and 20.8% as well. Moreover, it is noteworthy that DINO-DETR performs poorly when $N > 500$. Under these circumstances, there might be over 900 instances in some of the images, which is beyond the detection capability of DINO-DETR. In dense images, the detection limitation of DINO-DETR with only 900 queries will lead to many objects undetected (FN), resulting in a lower AP. Our DQ-DETR dynamically selects more queries for dense images, remarkably surpassing the baseline by 42.1% in terms of AP_{vt} .

4.5.3 Ablation of Categorical Counting Module.

Table 6 demonstrates the accuracy of the classification task in our categorical counting module. The performance is analyzed under four situations, where N is the number of instances per image. The total classification accuracy is about 94.6%, which means our categorical counting module can accurately estimate the number of objects N in the images. Furthermore, we can find that our categorical counting module has a poor classification performance with only 56.6% accuracy in the $N > 500$ situation since the number of training images is much fewer in this situation. Also, we observe that there are at most 2267 instances per image in the AI-TOD-V2 dataset. However, the long-tail distribution of the training samples restricts us from classifying the number of instances N per image in more detail. We have no choice but to categorize the images with $500 < N \leq 2267$ into the same class.

Table 5: **Evaluation results with different numbers of instances in the images.** K indicates the number of instances in the image, we separate the AI-TOD-V2 dataset into 4 classes based on K. All models are trained on the AI-TOD-V2 *trainval* split and evaluated on *test* split.

Model	#objects in image	#Query	AP	AP ₅₀	AP ₇₅	AP _{vt}	AP _t	AP _s	AP _m
DINO-DETR [6]	$N \leq 10$	900	22.5	53.1	14.8	10.6	24.5	25.7	34.9
	$10 < N \leq 100$	900	24.4	58.8	15.9	13.0	22.9	31.5	37.3
	$100 < N \leq 500$	900	31.6	67.3	26.9	10.1	25.4	39.6	38.2
	$500 < N$	900	13.5	27.9	7.3	5.7	6.4	34.7	32.4
	Overall	900	25.9	61.3	17.5	12.7	25.3	32.0	39.7
DQ-DETR(ours)	$N \leq 10$	300	26.1	60.4	19.7	12.7	29.6	28.5	40.8
	$10 < N \leq 100$	500	28.4	65.9	20.1	15.2	27.8	34.7	41.8
	$100 < N \leq 500$	900	33.7	69.9	30.4	11.1	30.4	42.0	41.6
	$500 < N$	1500	14.7	35.6	7.5	8.1	7.8	37.5	40.4
	Overall	dynamic	30.2	68.6	22.3	15.3	30.5	36.5	44.6

As for the detection accuracy, our DQ-DETR outperforms the baseline under all situations. The performances surpass the baseline by 16%, and 16.4% in terms of AP for $N \leq 10$, $10 < N \leq 100$. Nevertheless, our DQ-DETR performs slightly better than the baseline for the $N > 500$ scenario. This phenomenon is due to the poor classification accuracy for $N > 500$. The incorrect prediction from the categorical counting module will directly affect the number of object queries used for detection, where the inappropriate number of queries might harm the detection performance.

Table 6: The classification accuracy of our categorical counting module and detection accuracy of DQ-DETR with different numbers of instances in the images. DINO-DETR is compared as the baseline.

#Objects in image	Accuracy(%)	AP (DQ-DETR)	AP (Baseline)	#Sample
$N \leq 10$	97.7	26.1 (+3.6)	22.5	8674
$10 < N \leq 100$	90.5	28.4 (+4.0)	24.4	4393
$100 < N \leq 500$	86.5	33.7 (+2.1)	31.6	905
$500 < N$	56.5	14.7 (+1.2)	13.5	46
Total	94.6	30.2	25.9	14018

Table 7: Ablation of using regression or classification in categorical counting module.

Method	AP	AP _{vt}	AP _t	AP _s	AP _m
Baseline	25.9	12.7	25.3	32.0	39.7
Regression	14.9	5.2	16.3	19.9	14.3
Classification	30.2	15.3	30.5	36.5	44.6

Table 7 compares our DQ-DETR’s performance of using classification or regression in the categorical counting module. The traditional crowd-counting methods usually regress the predicted counting number to a specific value. However, in our study, we use a classification head instead. This experiment demonstrates our DQ-DETR performance with these two methods. For the classification task, we classify the images into 4 classes and apply different numbers of queries in the transformer decoder, as we mentioned in the previous section. For the regression task, we regress an integer directly to predict the number of objects in the images and select the object queries corresponding to the predicted result.

The results demonstrate that using regression as a counting method performs extremely poorly. We impute the drastic performance drop for the following reasons: (1) It is challenging to regress an accurate number since the number of instances per image may vary significantly from 1 to 2267 in the AI-TOD-V2 dataset. (2) The unstable regression result will largely affect the number of queries used in the transformer decoder and cause the DETR model hard to converge.

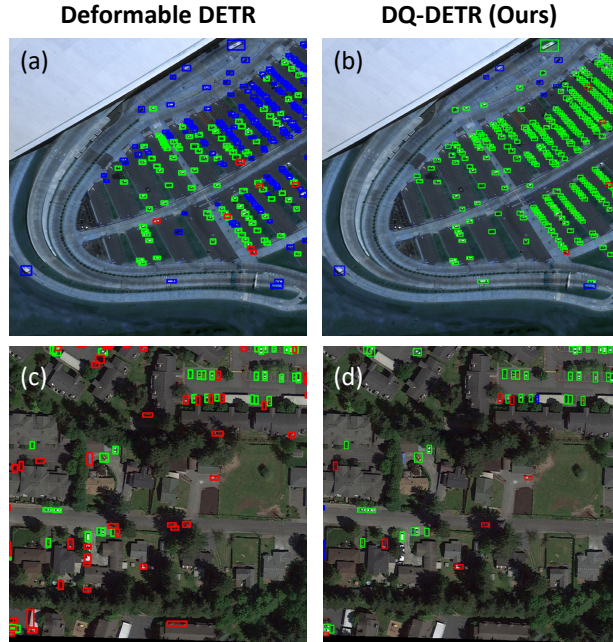


Figure 2: Visualization of detection results on AI-TOD-V2 dataset. (a) and (c) denotes the detection results of Deformable-DETR, while (b) and (d) denotes the detection results of our DQ-DETR. The green, red, and blue boxes represent TP, FP, and FN, respectively.

Owing to the above reasons, we believe that classifying how many objects exist in the image into different levels is a simpler way in contrast to regression. Thus, we take classification instead of regression as a preferable method in our proposed categorical counting module.

4.6 Visualization

Fig. 2 visualizes the detection results of Deformable-DETR compared with our DQ-DETR under sparse and dense situations. Deformable-DETR applies a fixed number ($K=300$) of queries, suffering a low recall rate under the imbalanced situation. The fixed number of queries will cause low detection accuracy in aerial datasets since the number of objects may vary drastically in different images. Using a small K restricts the recall of the objects in dense images, leaving lots of instances undetected (FN), as shown in Fig. 2(a). Conversely, Fig. 2(c) shows using larger K in the sparse images introduces many underlying false positive samples (FP).

5 Conclusion

In this paper, we analyze that the fixed number and position of queries in previous DETR-like methods are unsuitable for aerial datasets and propose a new end-to-end transformer detector DQ-DETR with categorical counting module, counting-guided feature enhancement, and dynamic query selection. Our DQ-DETR dynamically adjusts the number of object queries used for detection to solve the imbalance number of instances between different aerial images. Also, we improve the positional information of queries, making the decoder easier to localize the tiny object. DQ-DETR is the first DETR-like model focusing on tiny object detection and achieves 30.2% AP, which is the state-of-the-art of AI-TOD-V2. The result shows that our proposed DQ-DETR improves the performance of detecting tiny objects, outperforming all previous CNN-based detectors and DETR-like methods on the AI-TOD-V2 dataset with ResNet50 as the backbone.

6 Supplementary

6.1 Quantitative Result

6.1.1 FP/FN Under Different Density Situation

In table 8, we explore our DQ-DETR’s performance under different density situations, including sparse and dense images. We classify images with less than 100 objects as sparse and images with over 900 objects as dense. LRP FP and LRP FN [30] are used as the evaluation metric. Unlike AP metrics, a lower LRP value implies better performance. Previous DETR-like models apply a fixed number of object queries, while our DQ-DETR uses a dynamic number of queries depending on the object’s density in the picture.

DINO-DETR uses a fixed number of 900 queries for detection, no matter whether in dense or sparse situations. The number of queries exceeds the number of objects in the sparse image and hence introduces many underlying false positive samples (FP). In contrast, for dense images, the number of queries DINO-DETR uses is far less than the number of objects in images, which is beyond the detection capability of DINO-DETR, leaving lots of instances undetected (FN) and causes a large LRP FN score. Our proposed DQ-DETR dynamically adjusts the number of queries used for detection, resulting in fewer FP in sparse images and fewer FN in dense images.

Table 8: LRP FP and LRP FN score under different density situations in AI-TOD-V2. DINO-DETR is compared as the baseline.

Method	Situation	LRP FP	LRP FN
DINO-DETR	Sparse	29.4	40.7
	Dense	36.8	75.1
DQ-DETR	Sparse	25.7	36.4
	Dense	35.4	51.5

6.1.2 Ablation of Categorical Counting Module

In categorical counting module, we categorize the the number of objects N per image into four levels, which are $N \leq 10$, $10 < N \leq 100$, $100 < N \leq 500$, and $N > 500$. We selected the numbers 10, 100, and 500 based on the AI-TOD-V2 dataset’s characteristics, i.e., the mean and standard deviation of the number of instances N per image. Further, we only classify the number of objects N into four levels due to the long-tail distribution of the training samples. For the $N > 500$ situation, there are only 46 training images in this situation, which is much fewer than other cases and leads to a poor classification performance with only 56.6% accuracy. Although there are at most 2267 instances per image in the AI-TOD-V2 dataset, the long-tail distribution of the training samples restricts us from classifying the number of instances N per image in a more detail manner.

Table 9 and Table 10 demonstrates the detection performance and the accuracy of the classification task in our categorical counting module. We can observe that if we classify the the number of objects N into more classes, e.g. 5 classes, AP drops 1.4 compared to 4 classes situation. That is because the poor classification results from the categorical counting module will directly affect the number of object queries used for detection and the inappropriate number of queries might harm the detection performance. For 5 classes classification, while the total classification accuracy maintains 93.8%, the accuracy in the $500 < N \leq 900$, and $N > 900$ situations are only 37.1% and 57.4%. Since there are only few training images, the categorical counting module doesn’t perform well in these two situations and further impacts the detection performance. Hence, we only categorize the the number of objects N per image into four levels without partition the $N > 500$ situation into more detailed settings.

6.2 The categorical counting module (CCM) is dataset distribution-depend.

Since the characteristics of different datasets may vary a lot, it is vital to tailor our categorical counting module depending on the dataset property and determined how many queries should be used for object detection. In categorical counting module for AI-TOD-V2, we estimate the counting number N , i.e., the number of instances per image, by a classification head and categorize them into four levels, which are $N \leq 10$, $10 < N \leq 100$, $100 < N \leq 500$, and $N > 500$. It is worth noting that the hyperparameters 10, 100, 500 is tailored for AI-TOD-V2. For other datasets, the

Table 9: Ablation of categorical counting module. DINO-DETR is compared as the baseline.

Method	AP	AP _{vt}	AP _t	AP _s	AP _m
Baseline	25.9	12.7	25.3	32.0	39.7
Classification (4cls)	30.2	15.3	30.5	36.5	44.6
Classification (5cls)	28.8	14.3	29.2	34.1	43.1

Table 10: The classification accuracy of our categorical counting module with different numbers of classes.

#Objects in image	Accuracy(%) @ 4cls	Accuracy(%) @ 5cls	#Sample
$N \leq 10$	97.7	97.5	8674
$10 < N \leq 100$	90.5	89.3	4393
$100 < N \leq 500$	86.5	83.2	905
$500 < N \leq 900$	56.5	37.1	35
$900 < N$	-	54.4	11
Total	94.6	93.8	14018

hyperparameters used in the CCM can be pipelined into a logical process using the mean and variance of the objects per image in the dataset to avoid long-tail distribution. There is no need to hand-design the CCM for different datasets.

Algorithm 1 Categorical Counting Pseudo Code

```

1: function CATEGORICAL-COUNTING(features)
2:   mean  $\leftarrow$  Mean(dataset)
3:   var  $\leftarrow$  Variance(dataset)
4:   GT  $\leftarrow$  Predict(features)
5:   class1  $\leftarrow$  {GT < mean - var}
6:   class2  $\leftarrow$  {mean - var  $\leq$  GT < mean}
7:   class3  $\leftarrow$  {mean  $\leq$  GT < mean + var}
8:   class4  $\leftarrow$  {GT  $\geq$  mean + var}
9: end function

```

6.3 Visualization

Fig. 3 visualizes the detection feature maps of our DQ-DETR compared with Deformable-DETR. We can observe that DQ-DETR generates a more informative feature to detect tiny objects. In comparison, the feature from Deformable-DETR lacks of instances information, which leads to many object undetected (FN). Also, since Deformable-DETR uses a lot of object queries whose positional information is not refined for detecting tiny objects, there are many false positive in the detection result.

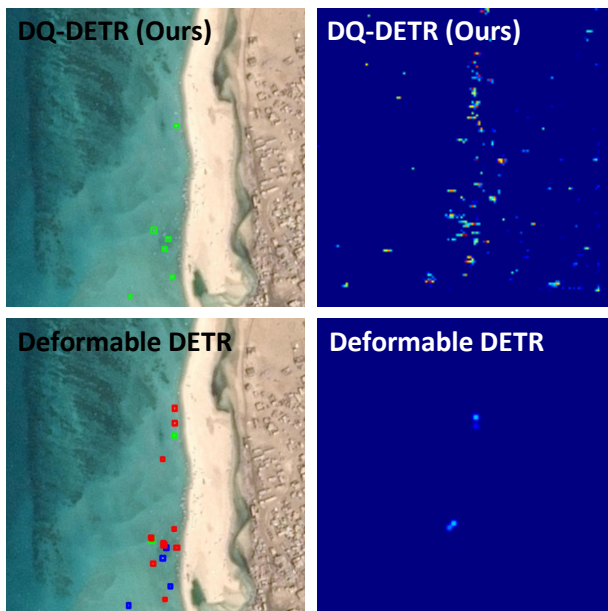


Figure 3: Visualization of detection results and feature maps. The green, red, and blue boxes represent TP, FP, and FN, respectively.

References

- [1] Shaoqing Ren, Kaiming He, Ross Girshick, and Jian Sun. Faster r-cnn: Towards real-time object detection with region proposal networks. *Advances in neural information processing systems*, 28, 2015.
- [2] Zhi Tian, Chunhua Shen, Hao Chen, and Tong He. Fcos: Fully convolutional one-stage object detection. In *Proceedings of the IEEE/CVF International Conference on Computer Vision (ICCV)*, October 2019.
- [3] Nicolas Carion, Francisco Massa, Gabriel Synnaeve, Nicolas Usunier, Alexander Kirillov, and Sergey Zagoruyko. End-to-end object detection with transformers. In *ECCV*, pages 213–229, 2020.
- [4] Xizhou Zhu, Weijie Su, Lewei Lu, Bin Li, Xiaogang Wang, and Jifeng Dai. Deformable detr: Deformable transformers for end-to-end object detection. In *International Conference on Learning Representations*, 2021.
- [5] Feng Li, Hao Zhang, Shilong Liu, Jian Guo, Lionel M Ni, and Lei Zhang. Dn-detr: Accelerate detr training by introducing query denoising. In *Proceedings of the IEEE/CVF Conference on Computer Vision and Pattern Recognition*, pages 13619–13627, 2022.
- [6] Hao Zhang, Feng Li, Shilong Liu, Lei Zhang, Hang Su, Jun Zhu, Lionel M. Ni, and Heung-Yeung Shum. Dino: Detr with improved denoising anchor boxes for end-to-end object detection, 2022.
- [7] Shilong Liu, Feng Li, Hao Zhang, Xiao Yang, Xianbiao Qi, Hang Su, Jun Zhu, and Lei Zhang. DAB-DETR: Dynamic anchor boxes are better queries for DETR. In *International Conference on Learning Representations*, 2022.
- [8] Shilong Zhang, Xinjiang Wang, Jiaqi Wang, Jiangmiao Pang, Chengqi Lyu, Wenwei Zhang, Ping Luo, and Kai Chen. Dense distinct query for end-to-end object detection. In *CVPR*, pages 7329–7338, June 2023.
- [9] Chang Xu, Jinwang Wang, Wen Yang, Huai Yu, Lei Yu, and Gui-Song Xia. Detecting tiny objects in aerial images: A normalized wasserstein distance and a new benchmark. *ISPRS Journal of Photogrammetry and Remote Sensing*, 190:79–93, 2022.
- [10] Zhiqing Sun, Shengcao Cao, Yiming Yang, and Kris M. Kitani. Rethinking transformer-based set prediction for object detection. In *Proceedings of the IEEE/CVF International Conference on Computer Vision (ICCV)*, pages 3611–3620, October 2021.
- [11] Xiyang Dai, Yinpeng Chen, Jianwei Yang, Pengchuan Zhang, Lu Yuan, and Lei Zhang. Dynamic detr: End-to-end object detection with dynamic attention. In *2021 IEEE/CVF International Conference on Computer Vision (ICCV)*, pages 2968–2977, 2021.
- [12] Yingming Wang, Xiangyu Zhang, Tong Yang, and Jian Sun. Anchor detr: Query design for transformer-based detector. In *Proceedings of the AAAI Conference on Artificial Intelligence*, volume 36, pages 2567–2575, 2022.
- [13] Depu Meng, Xiaokang Chen, Zejia Fan, Gang Zeng, Houqiang Li, Yuhui Yuan, Lei Sun, and Jingdong Wang. Conditional detr for fast training convergence. In *Proceedings of the IEEE International Conference on Computer Vision (ICCV)*, 2021.
- [14] Mate Kisantal, Zbigniew Wojna, Jakub Murawski, Jacek Naruniec, and Kyunghyun Cho. Augmentation for small object detection. *arXiv preprint arXiv:1902.07296*, 2019.
- [15] Barret Zoph, Ekin D Cubuk, Gholnadj Ghiasi, Tsung-Yi Lin, Jonathon Shlens, and Quoc V Le. Learning data augmentation strategies for object detection. In *European conference on computer vision*, pages 566–583. Springer, 2020.
- [16] Jinwang Wang, Chang Xu, Wen Yang, and Lei Yu. A normalized gaussian wasserstein distance for tiny object detection. *arXiv preprint arXiv:2110.13389*, 2021.
- [17] Chang Xu, Jinwang Wang, Wen Yang, Huai Yu, Lei Yu, and Gui-Song Xia. Rfla: Gaussian receptive field based label assignment for tiny object detection. In *European conference on computer vision*, pages 526–543. Springer, 2022.
- [18] Chang Xu, Jinwang Wang, Wen Yang, and Lei Yu. Dot distance for tiny object detection in aerial images. In *Proceedings of the IEEE/CVF Conference on Computer Vision and Pattern Recognition*, pages 1192–1201, 2021.
- [19] Seyed Hamid Rezaatofghi, Nathan Tsoi, JunYoung Gwak, Amir Sadeghian, Ian D. Reid, and Silvio Savarese. Generalized intersection over union: A metric and a loss for bounding box regression. In *Proceedings of the IEEE Conference on Computer Vision and Pattern Recognition*, pages 658–666, 2019.
- [20] Tsung-Yi Lin, Priya Goyal, Ross Girshick, Kaiming He, and Piotr Dollar. Focal loss for dense object detection. *IEEE Transactions on Pattern Analysis and Machine Intelligence*, 42(2):318–327, 2020.
- [21] Jinwang Wang, Wen Yang, Haowen Guo, Ruixiang Zhang, and Gui-Song Xia. Tiny object detection in aerial images. In *ICPR*, pages 3791–3798, 2021.

-
- [22] Joseph Redmon and Ali Farhadi. Yolov3: An incremental improvement. *arXiv preprint arXiv:1804.02767*, 2018.
 - [23] Zhaowei Cai and Nuno Vasconcelos. Cascade r-cnn: Delving into high quality object detection. In *Proceedings of the IEEE Conference on Computer Vision and Pattern Recognition (CVPR)*, June 2018.
 - [24] Siyuan Qiao, Liang-Chieh Chen, and Alan Yuille. Detectors: Detecting objects with recursive feature pyramid and switchable atrous convolution. In *Proceedings of the IEEE/CVF Conference on Computer Vision and Pattern Recognition (CVPR)*, pages 10213–10224, June 2021.
 - [25] Tsung-Yi Lin, Piotr Dollár, Ross B. Girshick, Kaiming He, Bharath Hariharan, and Serge J. Belongie. Feature pyramid networks for object detection. In *Proceedings of the IEEE Conference on Computer Vision and Pattern Recognition*, pages 936–944, 2017.
 - [26] Glenn Jocher, Ayush Chaurasia, Alex Stoken, Jirka Borovec, NanoCode012, and Yonghye Kwon. YOLOv5: SOTA Realtime Instance Segmentation, November 2022.
 - [27] B. Du, Y. Huang, J. Chen, and D. Huang. Adaptive sparse convolutional networks with global context enhancement for faster object detection on drone images. In *2023 IEEE/CVF Conference on Computer Vision and Pattern Recognition (CVPR)*, pages 13435–13444. IEEE Computer Society, jun 2023.
 - [28] You Ma, Lin Chai, and Lizuo Jin. Scale decoupled pyramid for object detection in aerial images. *IEEE Transactions on Geoscience and Remote Sensing*, 61:1–14, 2023.
 - [29] Pengfei Zhu, Longyin Wen, Dawei Du, Xiao Bian, Heng Fan, Qinghua Hu, and Haibin Ling. Detection and tracking meet drones challenge. *IEEE Transactions on Pattern Analysis and Machine Intelligence*, 44(11): 7380–7399, 2021.
 - [30] Kemal Oksuz, Baris Can Cam, Emre Akbas, and Sinan Kalkan. Localization recall precision (lrp): A new performance metric for object detection. In *Proceedings of the European Conference on Computer Vision (ECCV)*, pages 504–519, 2018.